RICE UNIVERSITY

Design, Construction, and Commissioning of the Exit Charge Detector for BNL-AGS Experiment 896

by

Kristofer K. Kainz

A Thesis Submitted
in Partial Fulfillment of the
Requirements for the Degree

Master of Arts

Approved, Thesis Committee:

William J. Llope, Faculty Fellow, Director
Department of Physics

Billy E. Bonner, Professor
Department of Physics

Stephen D. Baker, Professor
Department of Physics

Houston, Texas

December, 1997

Abstract

Design, Construction, and Commissioning of the Exit Charge Detector for BNL-AGS Experiment 896

by

Kristofer K. Kainz

The Exit Charge Detector (ECD) is used to determine the impact parameter of relativistic gold-gold interactions in BNL-AGS Experiment 896 by measuring the total charge of projectile-like particles in each collision. Results are presented from simulations which optimized the ECD's dimensions. The ECD was then constructed, and the hardware and the construction techniques used are described. Analyses of data from the operation of the ECD in heavy-ion collisions are discussed. These analyses indicated a significant amount of correlated noise in the experiment. A method to correct for this noise offline is discussed. Also, significant probabilities for the interaction of the beam with materials other than the target are investigated. Finally, plans to improve the detector for the coming Spring 1998 ^{197}Au run are discussed.

Acknowledgments

As the work leading up to this thesis reaches its conclusion, I would like to express my gratitude for the contributions of those both inside and outside the E896 Collaboration:

• to my thesis advisor, William J. Llope, who arranged to have the ECD designed and constructed at Rice, and thus provided me with a thesis topic and the opportunity to defend it. His ideas and suggestions have been essential throughout the course of this project;

• to him and to E896 spokespersons Hank Crawford (UC-SSL) and Tim Hallman (BNL), for their faith in my ability to complete and implement the ECD;

• to John W. Mitchell at NASA GSFC, who has both vast technical knowledge and seemingly limitless patience in sharing it with me. His ideas on the design, construction, and implementation of the detector have been indispensable;

• to the other 50 percent of Rice University's graduate student delegation to E896, Christopher Stokely, for his assistance in commissioning the ECD, and his review and critique of this work;

• to Harry Themann, for serving on the Bonner Lab staff long enough to produce the machine drawings, and to lend his assistance in constructing the ECD;

• to King Chan, for his work in machining the components of the ECD light integration volume;

• to Ramiro Debbe, for his advice on ECD commissioning and interpretation of the data, as well as his assistance with the correlations of the various detectors;

• to him and to Zoran Milosevich (CMU), for their development of the BVD vectoring code;

• to Elisabeth Mogavero, for accomplishing the seemingly impossible feats of navigating BNL's catacomb-like bureaucracy and abating my phobia of New Yorkers. For this I am especially grateful;

• to Stathes Paganis (UT-Austin), for his prompt response to my frequent, and frequently-inane, questions regarding GEANT;

• to Salvo Costa (INFN-Catania), for his extremely helpful advice and assistance on a variety of Fastbus data-acquisition matters;

• and to my other colleagues in E896, for their highly intellectual and technical support.

Contents

I. Impact Parameter Measurements in Heavy-ion Collisions

Relativistic heavy-ion collisions, such as those performed at Brookhaven National Laboratory's (BNL) Alternating Gradient Synchrotron (AGS), provide high baryon densities and high energy densities in nuclear collisions. These quantities are expected to increase as the impact parameter decreases, or as the event "centrality" increases. Centrality is measured by the impact parameter, which is defined classically as the distance of closest approach between the trajectories of the centers of mass of the beam ion and target ion. As the centrality increases, so does the likelihood of observing interesting nuclear physics. [1] Sensitive impact parameter measurements are thus an important part of successful heavy-ion experiments.

The primary goal of BNL-AGS Experiment 896 (E896) is to search for the H_0 dibaryon, a bound six-quark state predicted by the MIT Bag Model. [2] The H_0 is predicted to be a short-lived neutral particle, which decays weakly in one of several charged channels. The E896 detector geometry was optimized to detect the decay products of the H_0. Thus, the experiment can efficiently detect other short-lived strange neutral particles as well, such as the Λ, $\overline{\Lambda}$, and K^0_s. [3]

The production of these neutral strange particles increases with the number of nucleon-nucleon interactions, or as the beam-target collision becomes more central. To determine the impact parameter of a collision, an experiment must measure one or more quantities which are known to be correlated with the number of nucleon-nucleon interactions. One such quantity is the energy produced in the beam-target interaction

region, or the "participant" region. Where the beam and target ions overlap, their nucleons collide and produce new particles with velocities between that of the beam and target nuclei. The number of these produced particles (or, multiplicity) is a measure of the degree of beam-target overlap, and thus the impact parameter of each collision. [1, 4]

Another quantity related to the impact parameter is the size of the remnant of the beam nucleus after its interaction with the target nucleus, or the total mass of projectile-like fragments. This quantity is directly related to the number of noninteracting projectile nucleons which continue forward with velocities essentially the same as that of the noninteracting beam. As the spectator nucleons are outside the beam-target overlap region, the total charge in spectator fragments decreases as the area of the beam-target overlap region increases, and thus as the impact parameter decreases. [1, 4]

These approaches for measuring the impact parameter are complementary. The multiplicity of produced particles in the participant region is correlated with the "violence" of the collision. The total mass in spectator fragments is correlated, via geometry, with the impact parameter directly.

Two detectors are used in E896 to measure these two observables related to the impact parameter. The first of these, the multiplicity telescope (MLT), responds proportionally to the number of charged particles produced in the participant region.

The second detector, called the Exit Charge Detector (ECD), measures the total charge of projectile spectator fragments.

In this Thesis, simulations are described that were performed to optimize the design of the ECD. The resulting design parameters will be presented. The ECD hardware so implemented and the construction techniques employed are discussed in the following section. Finally, results from analyses of experimental data collected during the January 1997 gold run at the AGS will be presented to investigate the performance of the ECD for the measurement of the impact parameter in E896.

II. Introduction to Experiment 896 and the ECD

The ECD must be able to detect spectator-like charged particles with high efficiency, yet it should intercept as few produced particles as possible. The detector response should depend on the particle's charge, rather than on its momentum or energy loss. It must be resistant to radiation damage, as it will be exposed to gold ions at high rates over long running periods. Its dynamic range should be broad; that is, it should be able to detect everything from a singly-charged particle to a gold nucleus. Its response should be independent of the beam intensity. And, finally, the detector's response to charged particles should be independent of the location on the detector where they strike it.

To fulfill the above requirements, an ECD was simulated with an appropriately-sized Čerenkov radiator, placed inside a diffusely-reflective light integration volume.

A Čerenkov radiator is considered instead of a scintillator because plastic scintillator would sustain radiation damage far too quickly in the presence of 11.6 GeV/c/nucleon gold ions at rates of 10^5 Hz.

For Čerenkov detectors, the light output also depends on the particle's velocity. To make the detector more dependent on the charge, the index of refraction of the radiator should be maximized. Since the threshold Čerenkov velocity is given by $\beta_{th}=1/\eta$, where η is the index of refraction, a lower value of η provides a tighter range of particle velocities that will lead to Čerenkov radiation. The ECD's response would then be highly dependent upon velocity. Fused silica has a slightly lower index of refraction than natural quartz (1.458 versus 1.54), which would motivate the use of natural quartz as the ECD radiator. However, fused silica has several advantages over natural quartz, as described in section IV.

The light produced upon a particle's passage through the radiator is to be collected by photomultiplier tubes (PMTs) with high single-photoelectron resolution. To minimize the dependence of the ECD signal upon the location where the charged particle struck the radiator, four to six PMTs are to be used. The PMT bases must also have the capacity to measure large signals with a negligible sag in the upper dynode stages. The PMTs are to be positioned so that the PMT photocathodes do not collect Čerenkov photons directly from the radiator.

A sketch of the baseline ECD design is shown in Figure 1. Before discussing simulations performed to optimize the design and positioning of the ECD, basic concepts of the rest of E896 will be presented.

The detectors of E896 are placed on the C-5 line at the AGS. The detector layout and the path of the noninteracting beam are shown in Figure 2. Two detectors were placed in the beamline upstream of the target (and not shown in Figure 2) to provide beam trajectory and kinematics. The Beam Counters (BCs) are two vacuum chambers, each with a 200 μm thick piece of Čerenkov quartz read out by two photomultiplier tubes. The BCs provide the overall event timing, and establish that exactly one gold ion interacted with the target in an event. Between the BCs and the target are two Beam Vertex Detectors (BVDs). Each BVD is a four-plane drift chamber providing an x coordinate and a y coordinate of the incident beam.

The target is placed in the bore of a superconducting sweeper magnet with a 4.7-Tesla field. A tungsten collimator is just downstream of the target, also inside the sweeper bore. Placed between the target and the collimator is the MLT, which is composed of four scintillator plates covered with lead plates, read out by PMTs via optical fibers.

To reconstruct the H_0 and other strange neutral particles, E896 uses three detectors downstream of the target. The centerpiece tracking detector for E896 is the Distributed Drift Chamber (DDC), which is a 144-plane wire chamber. The Time-Of-Flight array (TOF) is a series of about 200 plastic-scintillator slats, each read out

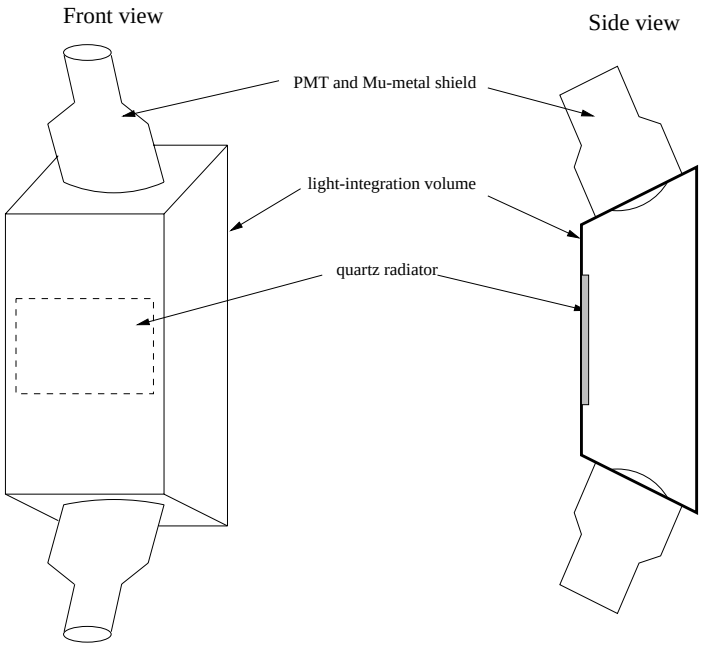

Figure 1: Shown here is a figurative drawing of the ECD, illustrating the relative locations of the radiator and the PMTs with respect to the light integration volume. The front surface of the ECD, within which the radiator is inset, faces the target. The top and bottom surfaces of the light integration volume are sloped, so that the photocathodes do not directly see light coming from the radiator.

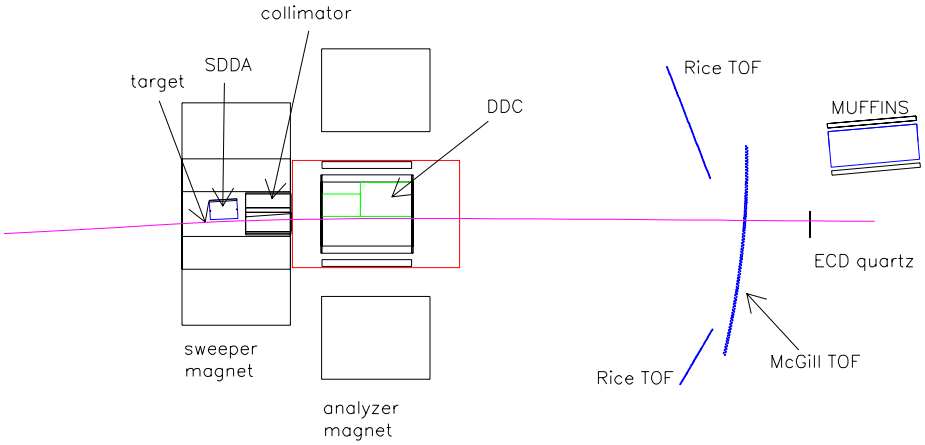

Figure 2: Top view of the E896 detector plan. The left-hand side of the picture is the upstream end of the cave; the beam is depicted hitting the ECD quartz radiator at the downstream end. Not shown are the beam counters and beam vertex detectors, which are both upstream of the target.

on the top and bottom ends by PMTs. It provides particle identification for DDC tracks via timing and space points for track reconstruction after a long flight path. Finally, a multi-functional neutron detector (MUFFINS) is behind the TOF array to detect the neutron from several of the anticipated decay schemes of the H_0.

III. Simulations to Optimize ECD Design

A. Modeling E896 and the ECD in software

GEANT-based Monte Carlo simulations were performed to determine the optimal size for the radiator and positioning of the ECD in E896. The sensitivity of the ECD response to the event impact parameter was also studied. These simulations are described in this section.

GEANT is a subroutine library developed at CERN [5] which is used to simulate high-energy and heavy-ion experiments and their performance in a realistic environment. An interactive version of GEANT was developed at the University of Texas for E896 [6] and used for the present simulations. Modifications of this code were made to store the information relevant to the ECD, such as the event impact parameter and the charge and position of each particle incident upon the radiator.

The total event multiplicity, as well as the species and initial momenta of all the particles in each event input to GEANT for the simulations, were obtained from the HIJET heavy-ion interaction model. [7] The HIJET model considers heavy ion reactions as a simple superposition of nucleon-nucleon collisions including rescattering

of the nucleons and produced particles. This model therefore does not generate fragments in the events. Thus, an "afterburner" was used [8] to produce spectator fragments from the noninteracting nucleons according to HIJET. Two different classes of HIJET+fragment events were used in the present simulations. One class consisted of events with impact parameter, b, ranging from zero to 4 fm. The other class of events included the full range of impact parameters.[1] These events are referred to in the experiment as "minimum bias."

These events were filtered through the experimental acceptance of E896 by using GEANT. The location and momentum of all particles striking the ECD radiator were stored, at the origin and at the radiator, along with their charge and the event impact parameter.

Each particle's contribution to the ECD response was calculated from its charge and the radiator thickness in the following manner. To associate a PMT response to an ECD radiator-incident charge, the Tamm-Frank representation for Čerenkov energy loss in a material was used. [9] The number of Čerenkov photons, $N_{C\gamma}$, generated per unit radiator thickness by a charged particle is given by,

$$\frac{dN_{C\gamma}}{dl} = 2\pi\alpha Z^2 \int_{\lambda_1}^{\lambda_2} \left[1 - \left(\frac{1}{\beta\eta}\right)^2\right] \frac{1}{\lambda^2} d\lambda, \tag{1}$$

provided that $\beta > \frac{1}{\eta}$. Here, the fine structure constant is α ($\approx \frac{1}{137}$), the charge of the ECD-incident particle in units of e is Z, the velocity of the ECD-incident particle is

[1] The radius of ^{197}Au is 7 fm, so the maximum impact parameter for gold-gold nuclear collisions is 14 fm.

β, the index of refraction of the radiator is η, and the lower and upper boundaries, respectively, of the range of detectable wavelengths are λ_1 and λ_2.

Assuming the radiator is non-dispersive,[2] the index of refraction is independent of the wavelength. Hence, Equation (1) can be integrated to yield,

$$\frac{dN_{C\gamma}}{dl} = 2\pi\alpha Z^2 \left[1 - \left(\frac{1}{\beta\eta}\right)^2\right] \left[\frac{1}{\lambda_1} - \frac{1}{\lambda_2}\right]. \tag{2}$$

RCA Burle 8854 PMTs are most sensitive to wavelengths from $\lambda_1 \approx 260$ nm to $\lambda_2 \approx 420$ nm. Incorporating this into equation (2) yields,

$$\frac{dN_{C\gamma}}{dl} = (672)Z^2 \left[1 - \left(\frac{1}{\beta\eta}\right)^2\right] \text{photons/cm}. \tag{3}$$

The PMT response is characterized by the number of photoelectrons, N_{pe}, generated in the photocathode. To associate N_{pe} to $N_{C\gamma}$, efficiencies are assumed for the quantum efficiency of photon conversion in the photocathode (ϵ_{qe}), the photon reflectivity in the light integration volume (ϵ_{box}), and the photon loss due to the photocathodes' recession from the light integration volume (ϵ_{recess}).

The quantum efficiency of the photocathodes ϵ_{qe} was taken to be 24 percent, a few percent lower than the 27 percent quoted by RCA. [10] The photon collection efficiency, ϵ_{box}, may be estimated by a "white box" formula, $\epsilon = \frac{\kappa}{\kappa + a}$, where κ is the ratio of the photocathode area to the reflector area of box, and a is the absorption

[2] According to Corning's data sheet, there is a monotonic dependence of η on λ, where η ranges from 1.51 to 1.47 for the assumed wavelength range. For these extreme values of η, the difference between the corresponding photon yields is about 4 percent. We therefore ignore dispersion in the description of the production of Čerenkov light.

coefficient of the reflector. Estimating κ to be 12 percent from the baseline ECD's dimensions, plus a 5 percent absorption in the reflector, [11] yields a light-collection efficiency, ϵ_{box}, of 71 percent. Finally, the quantity ϵ_{recess} was assumed to be 78 percent. Thus, $N_{pe} = \epsilon_{qe}\epsilon_{box}\epsilon_{recess}N_{C\gamma} = (0.13)N_{C\gamma}$. Folding the above efficiencies with Equation (3) gives the ECD PMT response per unit thickness of radiator to be,

$$\frac{dN_{pe}}{dl} \approx 90Z^2 \left[1 - \left(\frac{1}{\beta\eta}\right)^2\right] \text{ photoelectrons/cm.} \tag{4}$$

For each event, the total ECD signal, S, is the sum over all ECD hits, i.e.,

$$S = \sum_{i=1}^{N_{hits}} N_{pe}^{(i)}(Z_i, \beta_i), \tag{5}$$

where N_{hits} is the number of charged particles striking the ECD radiator in an event, and,

$$N_{pe}(Z_i, \beta_i) = 90Z^2\Delta x \left[1 - \left(\frac{1}{\beta\eta}\right)^2\right] \text{ photoelectrons,} \tag{6}$$

with Δx being the thickness of the radiator in centimeters.

B. Results of simulations

The ECD must be capable of detecting all projectile-like fragments produced over the full range of impact parameters. If a fragment from a high impact parameter event misses the ECD, there would be less Čerenkov radiation emitted then expected, and that event would be mistakenly regarded as having a low impact parameter. At the

same time, the radiator area should not be so large that many charged particles from the participant region are accepted.

In Figure 3, the number of photoelectrons calculated from Equation (6) is plotted versus the impact parameter of full gold-gold interaction events processed through GEANT. According to this figure, there are strong correlations between the impact parameter and the ECD signals of $A/Z \geq 2$ particles. Therefore, it is essential that the ECD collect all of these particles. Essentially no impact parameter information is carried by singly-charged particles. Thus, in optimizing the radiator size, the focus was only on efficiently collecting the alpha particles and heavy fragments.

Using an exceedingly large radiator in the simulation, the x distribution of the $A/Z = 2$ and $A/Z > 2$ particles striking the radiator is shown in the left-hand plot in Figure 4 for the $b < 4$ fm events. The x distribution for the minimum bias events is shown in the right-hand plot. To detect only the peak of the $A/Z = 2$ fragments, the left-hand graph of Figure 4 suggests a radiator extending from a local $x = -10$ cm to a local $x = 4$ cm, hence a total radiator width of 14 cm. To also effectively detect fragments from the high impact parameter events, the length of the radiator need only be extended to a local $x = 15$ cm. The simulations thus imply that the radiator must have a minimum total width of 25 cm. A 30 cm wide radiator was chosen to allow for any uncertainties in the magnetic fields, the ECD location, the beam incident angle, and the beam momentum in the actual experiment.

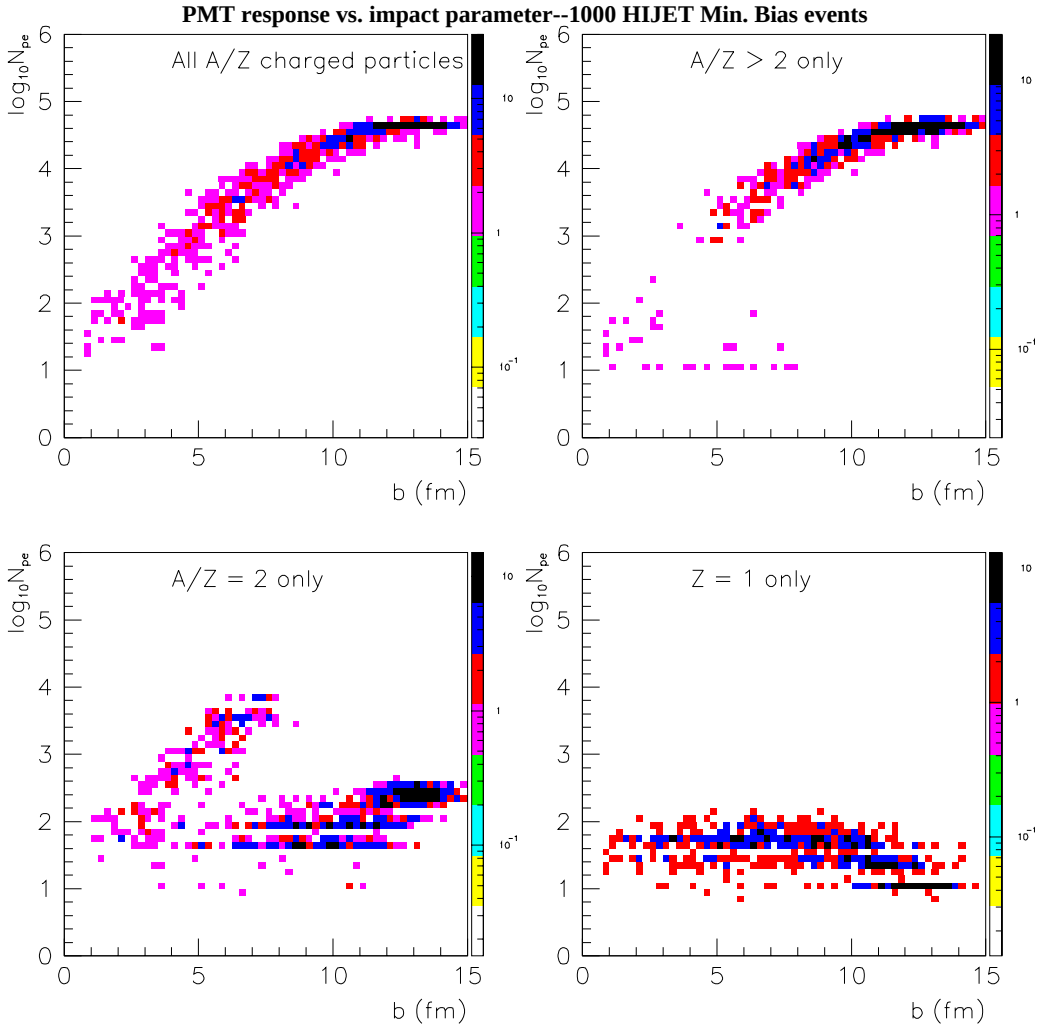

Figure 3: Shown here are plots of the number of photoelectrons produced per event versus the event impact parameter, for various cuts on A/Z. Note how the A/Z > 2 particles (heavy fragments) comprise almost all of the high-impact parameter signals, while the lower-impact parameter signals are due mostly to A/Z = 2 fragments (mostly alpha particles).

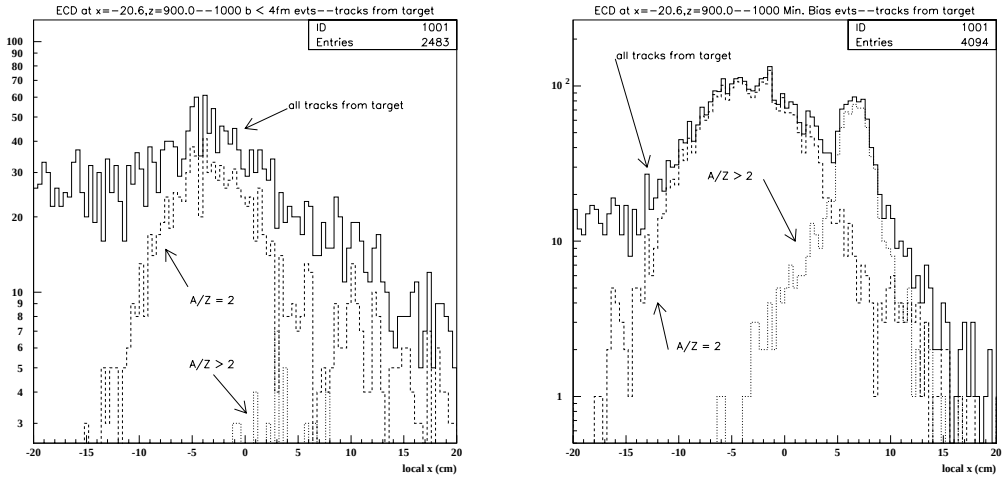

Figure 4: The left-hand graph shows the distribution of charged particles of target origin, plotted with respect to the local x coordinate of the radiator, for events with $b < 4$ fm. The right-hand graph shows the local x distribution for particles from minimum bias events.

Figure 5 depicts the y distribution of particles striking the oversized ECD in the simulations. According to this figure, the y distribution is more tightly correlated than the x distribution (see Figure 4). A Gaussian fit to the y distribution of the A/Z = 2 fragments, shown in Figure 6, yields a standard deviation of 2.9 cm. The minimum height of the radiator was chosen to be twice 3σ, or 17.4 cm. The final radiator height was chosen to be 20 cm, to allow for experimental uncertainties.

Simulations were then performed to determine the optimal height of the light integration volume (see Figure 1). If a particle were to strike one of the PMT photocathodes directly, the resulting signal would have little to do with the amount of light produced in the radiator, and thus give an incorrect measure of the total mass

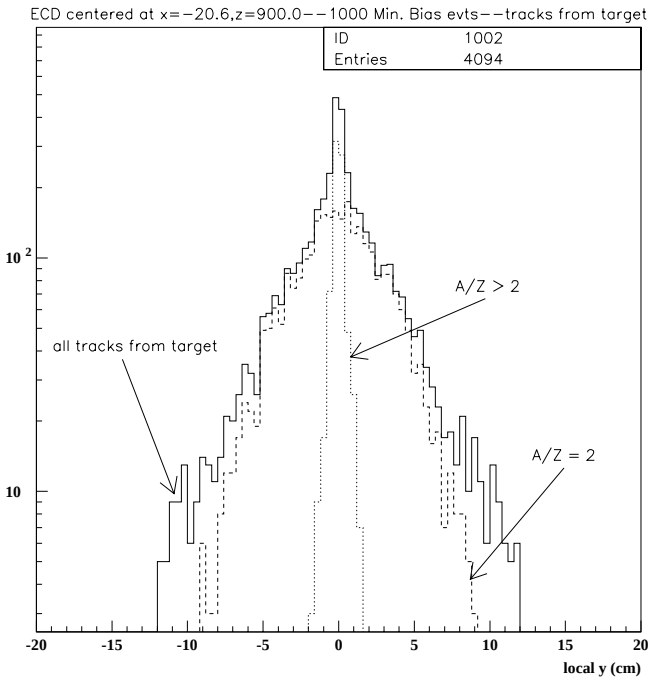

Figure 5: Distribution of charged particles of target origin, with respect to the local y coordinate of the radiator. Minimum bias events are used here.

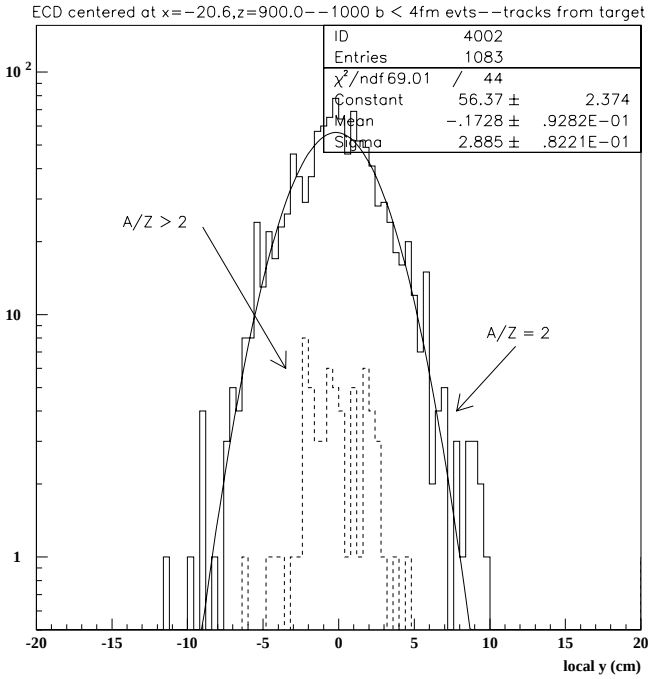

Figure 6: Distribution of charged particles of target origin, with respect to the local y coordinate of the radiator. Events such that $b < 4$ fm were used.

of projectile-like fragments. A high charged-particle flux would also damage the photocathodes as well. Therefore, the PMTs must be placed far enough above and below the beamline to limit the probability of a photocathode hit per central event to below 10 percent.[3] At the same time, however, the light integration volume should not be so large that too much Čerenkov light would be lost to absorption. This determined the height of the ECD front plate.

The photocathode-hit probability was defined in the following manner. First, the round photocathodes were approximated by rectangular bands, whose dimensions are given by the diameter of the photocathodes and the width of the ECD. Using Figure 7, which shows the y distribution of particles on the ECD front face, the photocathode-hit probability was determined by moving these rectangular bands farther from the center of the front plate until the probability of a photocathode hit reached an acceptably low level.

For a 20 cm front plate (the same height as the radiator), the probability of a photocathode hit in an event with impact parameter less than 4 fm is 46 percent. Considering only events with $b < 2.5$ fm, the photocathode-hit probability was 41 percent. To reduce the photocathode-hit probabilities to less than 10 percent of the relatively central events, the front-plate height must be a minimum of 60 cm. In the $b < 4$ fm events, the probability of a hit became 8.8 percent; among $b < 2.5$ fm events, it reduced to 7.2 percent.

[3]Ten percent was chosen to be the maximum photocathode-hit probability arbitrarily.

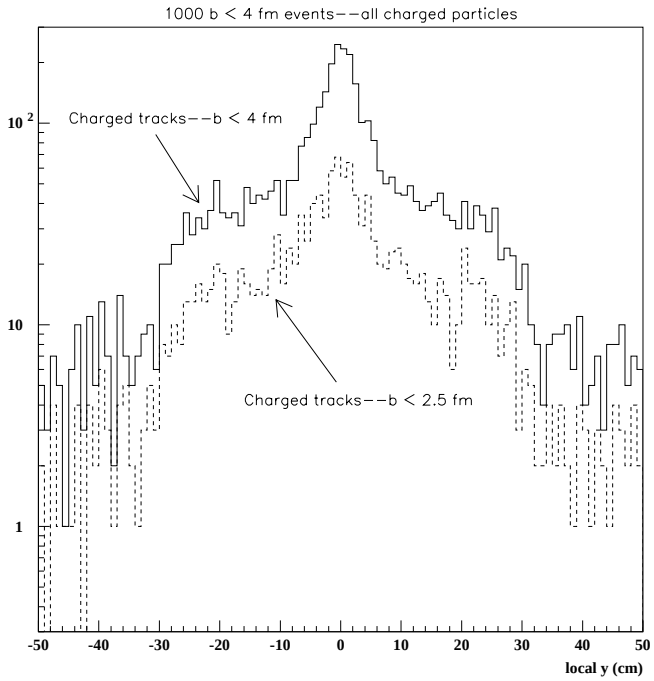

Figure 7: Shown here is a local y distribution of tracks from the target, with cuts on the impact parameter. The photocathode-hit probabilities were determined from this plot.

With the radiator dimensions and the height of the light integration volume so determined, the only remaining quantity to be extracted from the present simulations is the radiator thickness. For a thinner radiator, fewer secondaries would be produced in the radiator itself, and the likelihood of fragment dissociation in the radiator decreases. However, thinner radiators produce less light, resulting in a poorer resolution.

The radiator thickness was chosen such that an average of 10 photoelectrons are generated from a singly-charged particle.[4] According to Equation (6) and shown in Figure 8, a single Z=1 particle must pass through about 2 mm of quartz in order to generate ten photoelectrons on average. The probability of a gold-ion interaction with a 2 mm thick radiator is 4.3 percent.

After the quartz thickness was computed, the expected photoelectron yield from noninteracting gold ions was determined. The gold beam itself generates the largest PMT signal which the ECD must be capable of handling. Therefore, the maximum number of photoelectrons is expected to be $10^{4.8}$ per event. Thus, the required dynamic range of the bases is $10^{3.8}$, or about 6300.

Shown in Table 1 are all of the ECD design parameters extracted from the present simulations. In the following section, detailed information on the construction and commissioning of the ECD in E896 is presented.

[4]Given that the ECD PMTs have superb single photoelectron resolution, 10 photoelectrons per Z=1 hit were assumed to be sufficient.

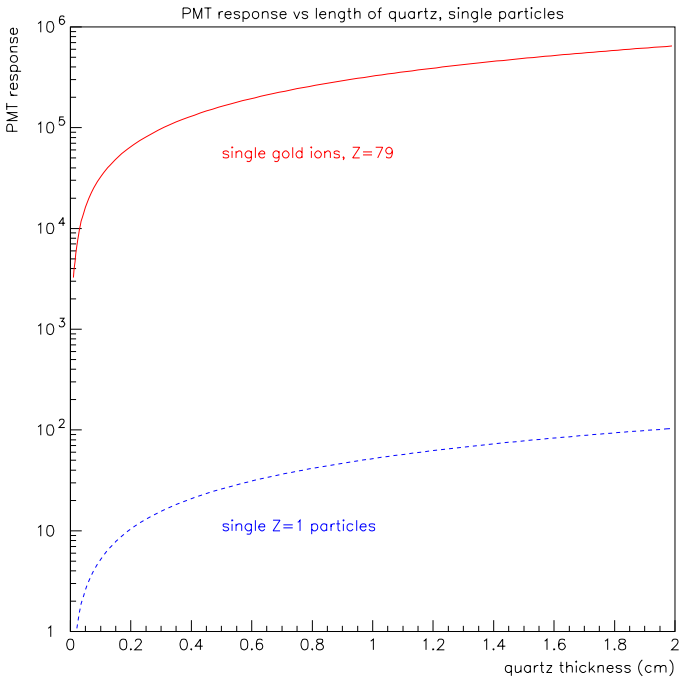

Figure 8: The PMT response, S, from Equation (6) is plotted as a function of the radiator thickness for gold ions and for singly-charged particles.

design parameter	*result*
radiator width	30 cm
radiator height	20 cm
front-plate height	60 cm
radiator thickness	2 mm
radiator center, GEANT-x	-11.7 cm
radiator center, GEANT-y	-1.2 cm
radiator center, GEANT-z	927.2 cm

Table 1: Shown here is an overview of the ECD design parameters determined by the simulations described above. The GEANT z-axis is the axis of the analyzer magnet; the downstream face of that magnet corresponds to z=500 cm. The GEANT y-axis gives the vertical coordinate; negative values correspond to distances below the GEANT z-axis. Negative values of GEANT-x correspond to distances to the right of the z-axis, looking downstream.

IV. ECD Construction and Electronics

A. Description of hardware used

The radiator used in the ECD was UV-grade fused quartz, Corning Code 7940. Although UV-grade quartz can be three times as expensive as commercial-grade quartz, it has two advantages. Its improved uniformity leads to better transmission of ultraviolet light than for commercial-grade; for 240 nm light, UV-grade has 90–95 percent transmittivity, versus 80–85 percent for commercial-grade quartz. Corning's data sheet states a 91 percent transmittivity for 240 nm light, increasing to about 93 percent for 420 nm light.

Also, there are fewer imperfections in UV-grade quartz around which irradiation can create "color centers." Such color centers optically darken the quartz, making it less transmissive.[5] According to Corning's data sheet, the 7940 fused quartz is suitable for use in space, "in manned space flights and for long term passive energy collectors." [12]

To reduce internal reflections within the radiator, the surfaces of the quartz were made coarse. This also makes the outgoing light more diffuse.

To gather the Čerenkov light, four RCA 8854 photomultiplier tubes were used, two on top and two on bottom. Four PMTs were used, instead of two, to minimize the dependence of ECD signals on the location of the hits on the radiator face. Some

[5]The effect is similar to that seen in deposits of "smoky quartz" found in the earth's crust, whose discoloration is brought about by radiation from rare-earth metals nearby.

qualities of the 8854s which made them appealing for use in the ECD are the 4.5 inch minimum diameter of the photocathodes, and their good quantum efficiency for shorter wavelengths (RCA quotes 27 percent for 400 nm). The glass covering of the photocathode has a high transmission of UV light. Also, they have good resolution for single-photoelectron events. This is due to the high gain in the first dynode stage. The PMTs have a fast (3 nsec) rise time, which is important for the use of the ECD as an event trigger. These PMTs have been successfully used in detectors in other experiments, such as the LBL Di-Lepton Spectrometer (DLS) and BNL E878.

The 8854s operate at higher voltages than those for smaller PMTs. Typically, 1900–2000 Volts is required to see dark current on the anode, while the maximum recommended voltage is 3500 Volts. The drift time of the electrons through all dynode stages is rather long, around 66 nsec at 3000 Volts.

A series of Zener diodes was placed between the photocathode and the first dynode. They hold the photocathode and first dynode at a constant potential difference of 800 Volts. This provides a constant gain for the first photomultiplier stage, regardless of how much in excess of 800 Volts the PMT is operated. Thus, the average number of photoelectrons produced in the first photomultiplier stage is independent of the overall PMT gain. This is useful for calibrating the ECD signals from the gold-beam runs to those from LED calibration tests and Z=1 test beams.

The PMT bases must be able to handle beam rates as high as 10^5 Hz. High rates can aversely affect the ECD performance by causing the voltage on the upper dynodes

to sag, which reduces the PMT gain slightly for the next event. So the degree to which the voltage on the dynodes can be held constant determines the rate capability of the ECD bases.

In the PMT-base hardware, high-permeability magnetic shields were used to prevent any loss of secondary-electron collection efficiency along the photomultiplier stages. Upon switching from the positive-high voltage bases to negative high-voltage bases,[6] the magnetic shields will also serve as electrostatic shields, since the outer can of the PMT will then be at high voltage.

To randomize the path taken by a photon from the point of its creation inside the radiator to the photocathode, the interior of the light integration volume was covered with tyvek. Tyvek is a white, fibrous paper, and is thus diffusive and highly reflective.

The sides of the box (with the exception of the top and bottom) must be strong enough to support the weight of the PMTs, bases, and shields, but light enough so as not to place too much strain on the ECD support structure. It must also be relatively low-mass so as not to interact with the beam. To avoid light leaks, it must also be opaque. For these purposes, 1/2 inch thick Gatorfoam was used. Gatorfoam is polystyrene foam, covered with about 1 mm thick sheets of Luxcell on both sides. Luxcell consists of wood fiber veneer with an admixture of resin to make the sheets resistant to moisture, small punctures, and warping. It can be painted with latex, oil-based, or acrylic paints, as well as the adhesive that was used to attach the tyvek.

[6]This is a planned upgrade which is described in the conclusion section.

The Gatorfoam can be shaped with standard machine tools. The top and bottom surfaces of the light integration volume were made out of 1 inch thick Delran, a strong, highly opaque, plastic-like, readily machinable compound.

Figure 9 illustrates how the ECD is mounted in E896. The ECD was hung from aluminum straps suspended from Unistrut segments which were attached to the support structure of the central TOF array.

B. Electronics and commissioning in the beam

The electronics chain used to process the ECD signals is shown in Figure 10. To digitize the analog signals, the LeCroy 1885F Fastbus ADC modules were used. The ECD was initially commissioned in the 11.6 GeV/c gold beam during the first week of January 1997, and was fully implemented into the E896 event trigger during the next three weeks afterward.

The voltage for each PMT was set such that its response to a gold nucleus incident upon the quartz resulted in a 500 mV pulse height. The raw anode pulses were each sent through an ORTEC 474 Timing Filter Amplifier, which amplified them by a factor of 20. The resulting amplified pulses were paired up (1 and 4, 2 and 3), and each pair was linearly summed using a LeCroy 428F linear fan. The result was sent to a Phillips 704 discriminator. Throughout the run, the discriminators for each sum of the two ECD amplified channels were set to their lowest value, which is 25 mV.

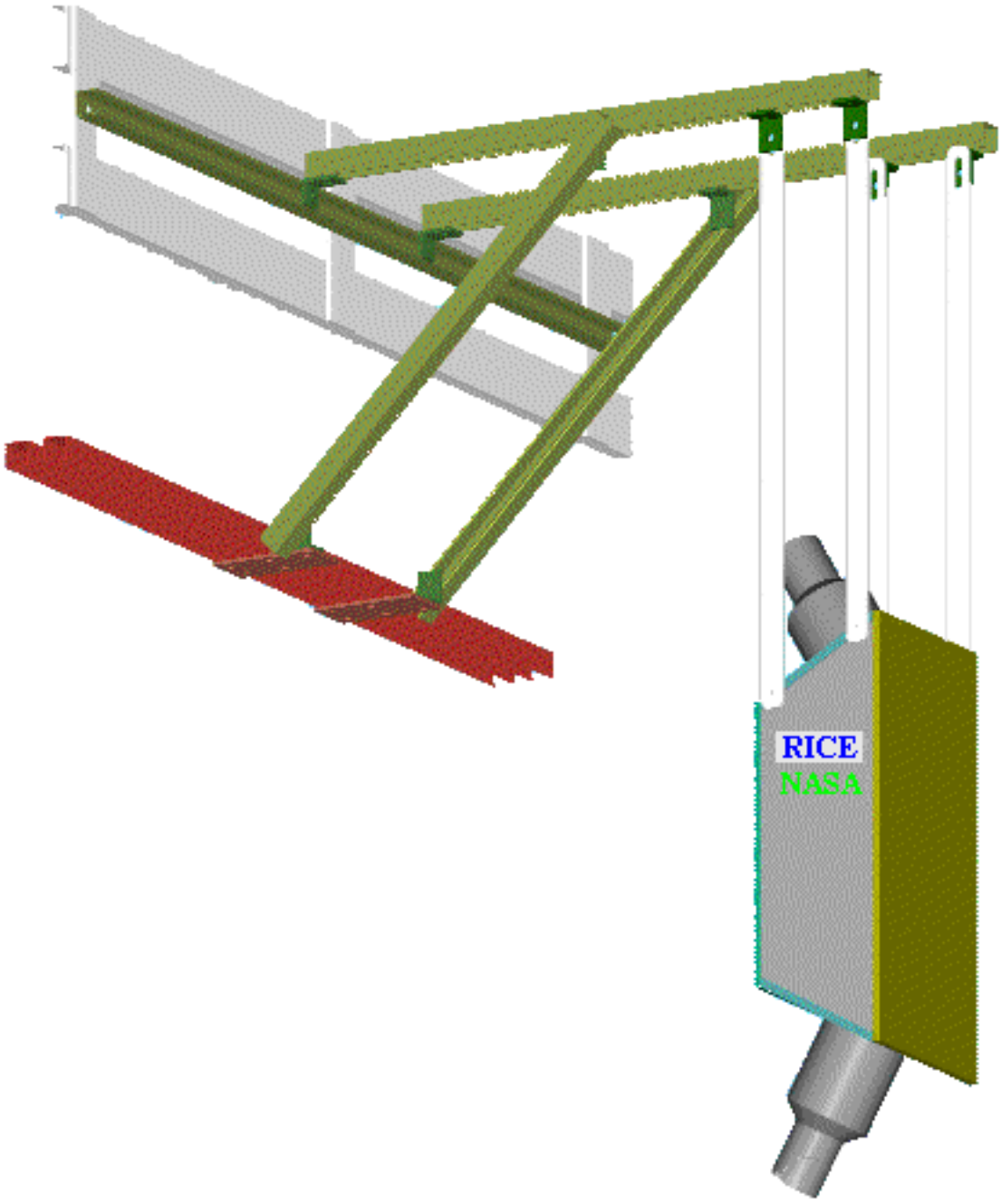

Figure 9: A 3-D AutoCAD drawing of the ECD and its support from the McGill TOF wall support structure. This is an accurate representation, except that there are two PMTs, side-by-side, on the top and bottom plates instead of just one.

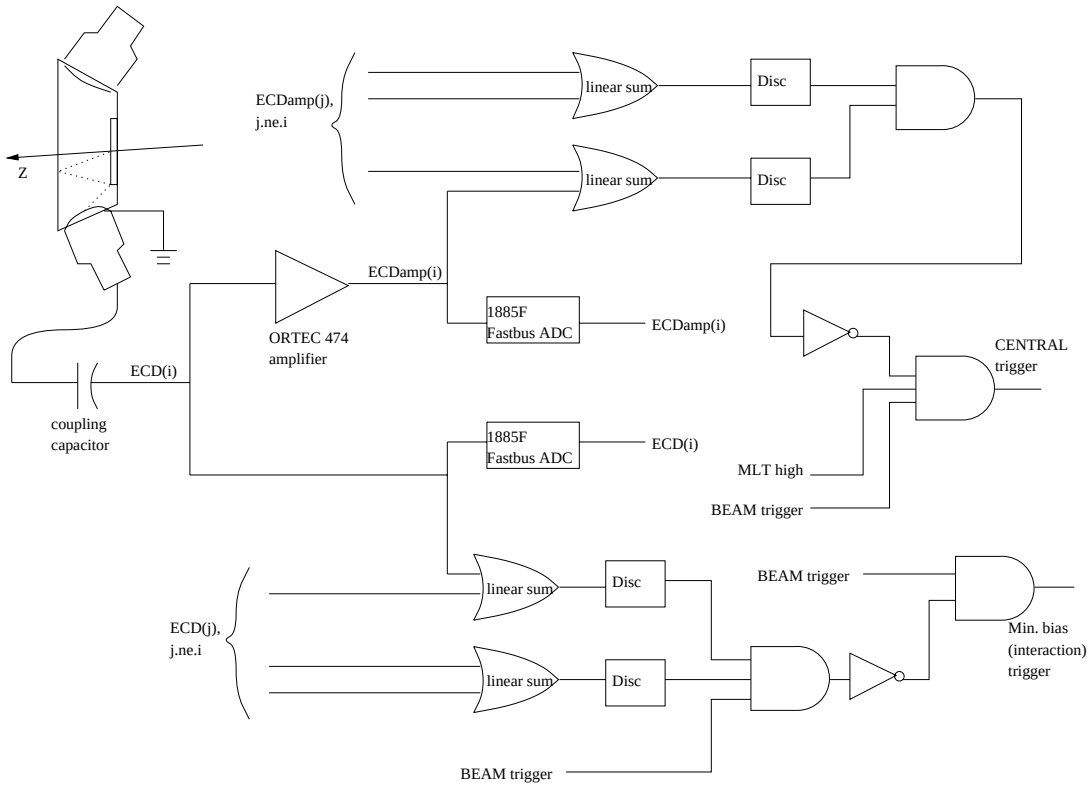

Figure 10: Shown here is a schematic of the use of the ECD in the E896 trigger system.

Data were taken from interactions between an 11.6 GeV/c/nucleon ^{197}Au beam and a ^{197}Au foil target. Three different target conditions were used: a 10% target,[7] a 5% target, and an empty target[8] to normalize the data.

Several event triggers have been implemented so as to write to tape the detectors' data for events fulfilling a particular range of impact parameters. Pulser-trigger events are performed when the beam is off. These are used to investigate noise in the detectors. Beam-trigger events are those in which one and only one gold ion approaches the target; this is the least-discriminating event trigger that is used when the beam is on. Central-trigger events involve low impact parameter cuts on the beam triggers.

One of the requirements for a central-event trigger is that at least one of the sums of the pairs of amplified ECD signals must not exceed the discriminator threshold. The other two are that the beam counters must indicate that one and only one gold ion came through in an event (beam trigger), and that all MLT channels must exceed a discriminator threshold. When these conditions are met, the interaction is considered to have low impact parameter, and the data from all detectors is written to tape.

Data from the January 1997 gold-ion run will be used to evaluate the ECD's performance in an actual experiment, and to establish its capability for measuring the impact parameter. These analyses are described in the following section.

---

[7] An "x% target" is such that a projectile gold ion has an x percent chance of interacting with it, using the geometrical cross section.

[8] Also designated as "MT target" or "T0" (target out).

V. ECD Analyses

> "I don't care about what something was *designed* to do, I care about what it *can* do."—Gene Kranz, *Apollo 13*

In this section, analyses of data collected using the ECD in the actual experiment are described. The primary goal is to determine whether or not the ECD performance is sensible, and to determine if any improvements to the ECD design are necessary in preparation for the Spring 1998 ^{197}Au run.

A. Interpretation of ECD output

Shown in Figure 11 are the spectra of ADC values obtained from each of the four ECD PMTs during a beam-trigger run with a 10% target. Each of the spectra from the individual PMTs is very similar. At low ADC values, there exists a small peak referred to as the "pedestal." The pedestal is comprised of ADC values from the detector when no particle strikes it. At high ADC values, a peak exists which corresponds to the passage of ^{197}Au through the radiator.

The sum of the ECD channels was formed in the following manner. The average pedestal value was subtracted from each channel. That average was found by fitting a Gaussian function to the pedestal peak in each raw ECD spectrum. The ADC values for each channel were then scaled such that all four gold-peak centroids were equal. The four ECD ADC values were then added together to form the ECD sum, which is shown in Figure 12.

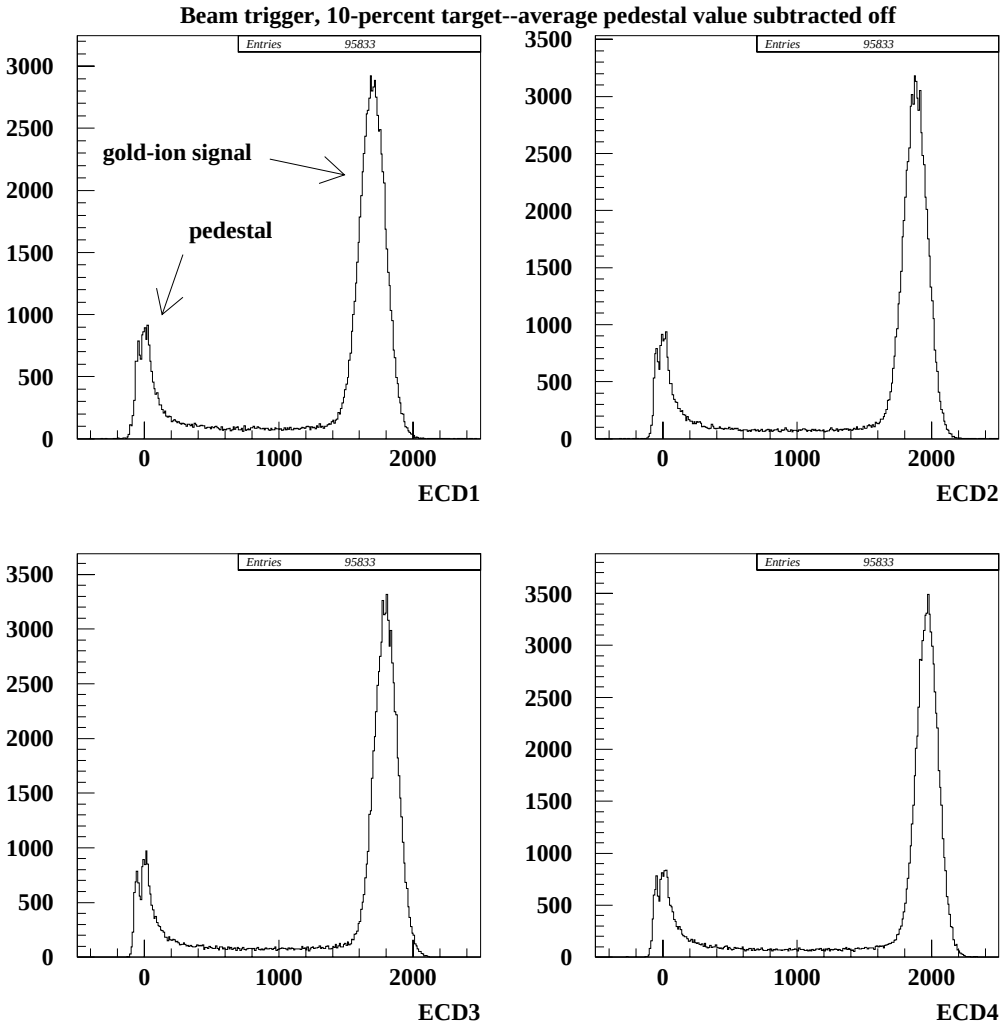

Figure 11: Raw ADC distributions from individual ECD PMTs, for beam-trigger events.

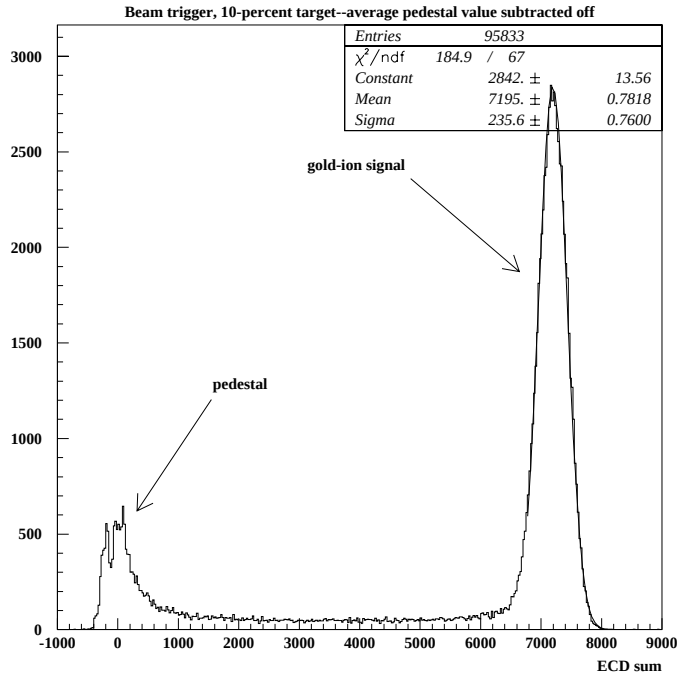

Figure 12: The sum of the ECD ADC channels is shown here for beam-trigger events, with the mean pedestal subtracted from each channel, and the gains matched. A Gaussian function is fit to the gold-ion signal peak. The parameters of the fit are shown at the upper right.

In the summed ECD signal distribution, two important effects are seen. First, the fraction of events in the gold-signal peak is 70 percent. However, for a "10% target" and a massless experiment, one would expect that the ECD response should be in the gold-signal peak 90 percent of the time. Therefore, interactions of the beam take place three times as often as one would expect for a gold projectile-gold target collision. This major discrepancy is one focus of the present analyses.

Second, individual peaks and a wide, non-Gaussian shape are seen in the pedestal, both for the individual ECD PMTs and for their sum. This suggests the presence of AC noise in the ADC signal lines. Shown in Figure 13 is the correlation of the sum of the ECD signals with the sum of the MLT signals. A strong correlation between the pedestal values in these two detectors is obvious. This suggests a large amount of correlated noise in the experiment.

The presence of correlated noise suggests that the ECD and MLT pedestals would each be tightly correlated with the ADC signal from a "blackened" PMT. Such a PMT is decoupled from all conceivable light sources, and thus is a direct measure of *only* the correlated noise. Described below is a technique to correct the ECD and MLT pedestals offline using the information obtained from a blackened PMT. After the correlated noise is removed, the question of the non-target interactions will be addressed.

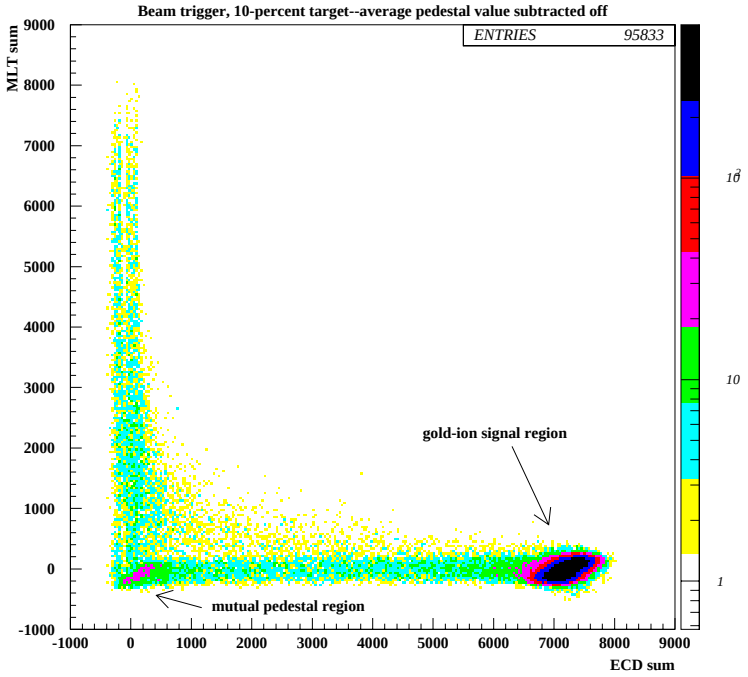

Figure 13: The sum of the MLT channels plotted against the sum of the ECD channels is shown here, for beam-trigger events. The overall average pedestal for each MLT and ECD channel was subtracted off. Note the correlations between the MLT and ECD values in the mutual pedestal region and the ECD gold-signal region.

B. Offline correction of correlated noise

Ground loops and other kinds of ill-advised electrical connections in the experiment result in noise in the data stream that affects all detectors. Optimally, these noise sources should be located and removed before data acquisition. In the January 1997 ^{197}Au run, the experiment was being commissioned, so the time and manpower to track down and remove the correlated noise was not available. In the present section, a technique for removing this noise offline will be described.

For a particular run, an event-by-event pedestal correction of the ECD and MLT signals was performed in the following manner. First, the ECD and MLT pedestal values were extracted from the raw data in that run. For each ECD and MLT channel, a "reference plot" was formed by plotting their pedestals against the blackened PMT ADC channel (hereafter referred to as "DSMON"[9]). The reference plots were then used in re-scanning the run. For each event, the DSMON ADC value was read, the ECD (or MLT) pedestal value corresponding to that DSMON value was obtained from the reference plot, and that ECD (or MLT) pedestal was subtracted from the raw ECD (or MLT) data value from that event.

The pedestals for each MLT channel were obtained from events in which the corresponding ECD value is in the gold peak. The pedestals for the ECD were obtained using "canary events"[10] that were interspersed with the beam-trigger data.

[9]This blackened PMT is part of the MUFFINS detector array.

[10]The canary was included as a diagnostic device to monitor the flow of helium-ethane gas into the DDC.

Shown in Figures 14 and 15 are examples of reference plots. Since the ECD-vs.-DSMON and MLT-vs.-DSMON correlations are not single-valued, the reference plots used in the pedestal correction algorithm took the form of profile histograms, such as those shown in Figure 15. In this way, an average ECD and MLT pedestal is defined versus the DSMON ADC value.

Shown in Figure 16 is the same correlation of MLT sum against ECD sum as in Figure 13, except that the event-by-event pedestal-correction algorithm was used. The technique dramatically narrowed the widths of the ECD and MLT pedestal peaks, and the correlation in the mutual pedestal region has been removed.

Using this pedestal correction technique also narrowed the width of the gold-signal peak in the ECD sum distribution, as seen in Figure 20. The ratio of the width to the mean following the correction was 2.8 percent, compared with 3.3 percent beforehand.

C. Investigation of beam interactions in E896 materials

With the noise in the ECD and MLT signal distributions removed offline, one may return to the non-target-interaction question raised earlier. According to Figures 12 and 17, only about 70 percent of the incident beams travel all the way to the ECD and result in a gold-like signal. For a 10% target, one should expect 90 percent of the events to accumulate in the gold-signal peak.

Presented first are the probabilities of beam interactions within the E896 beam-line that were determined by integrating the ECD gold-signal peaks and the MLT pedestal peaks obtained from the beam-trigger data. Results of calculations of the

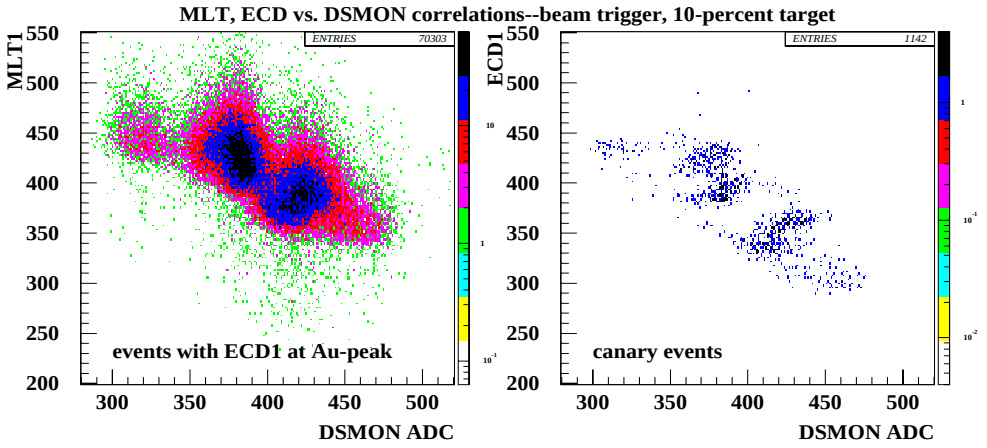

Figure 14: The left-hand plot shows the ADC signal from the first MLT channel versus the DSMON blackened PMT ADC value. The events used to compile the correlation plot were such that ECD1 was within the gold-signal peak. The plot of ECD1 pedestals versus DSMON is shown on the right. Canary events from the beam-trigger run were used to extract the ECD pedestals.

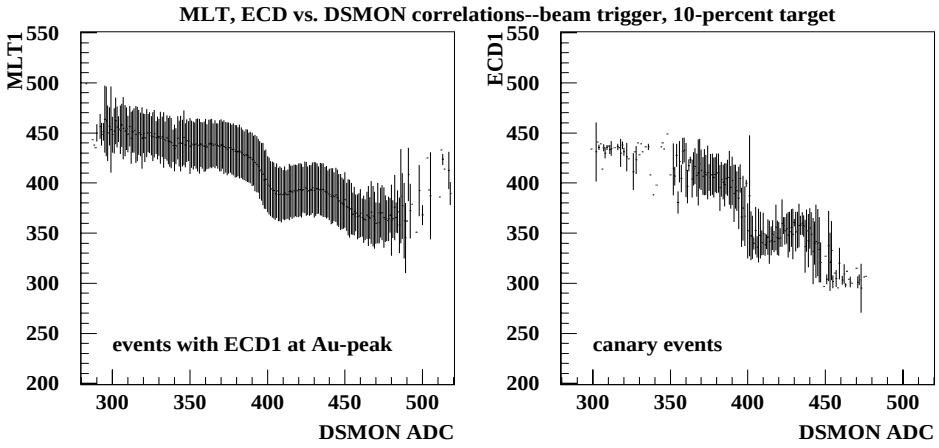

Figure 15: These are the same plots as in Figure 14, shown in profile histogram form.

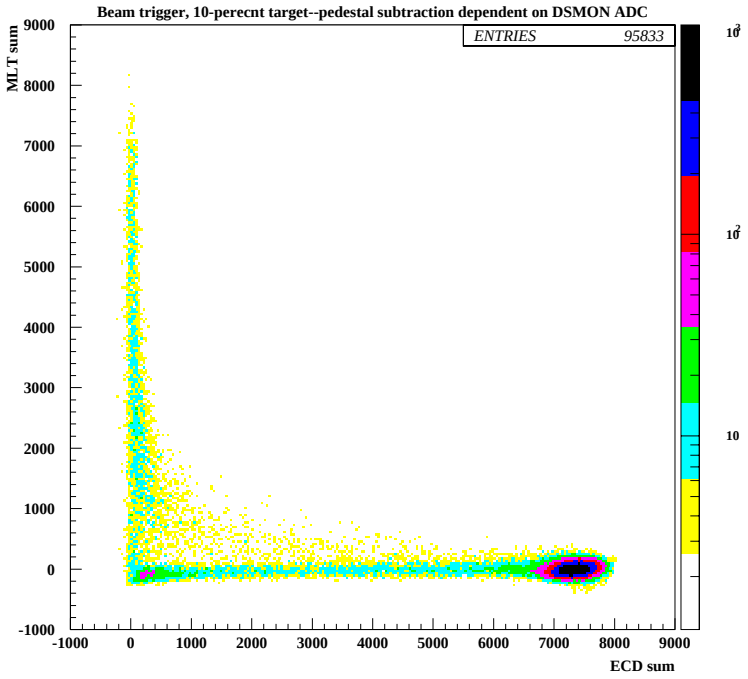

Figure 16: The sum of the MLT signals versus the sum of the ECD signals is plotted for beam-trigger events, after applying the event-by-event pedestal correction technique described in the text. The correlations in the mutual pedestal region and the gold-signal region are no longer visible.

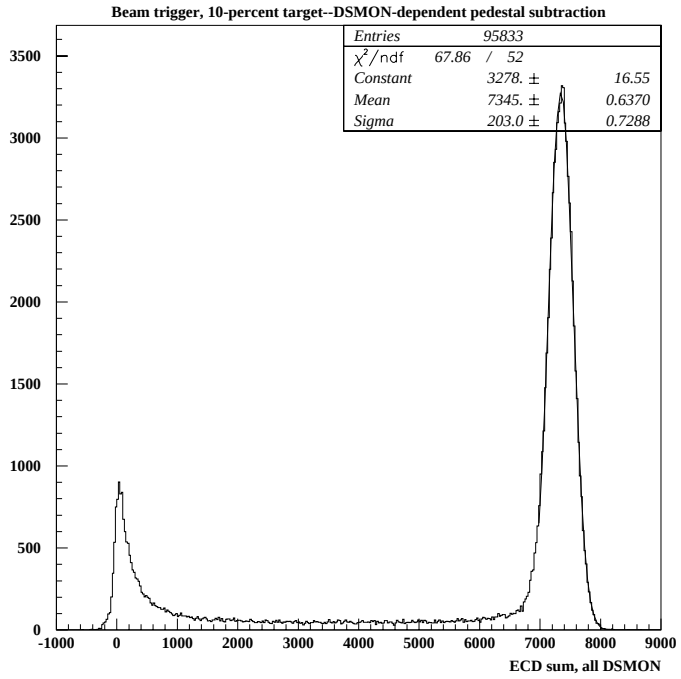

Figure 17: The sum of the ECD signals for beam-trigger events, using the event-by-event pedestal correction technique, is plotted above.

interaction probabilities between the beam and the various beamline elements will then be presented in order to account for these non-target interactions.

The overall beam survival probability is determined by counting the number of events in the gold-signal peak in the ECD data. The ECD signals below the gold-signal peak are due to beam interactions with the target and all beamline materials between the BCs and the ECD.

For the MLT distributions, beam interactions appear as ADC values greater than the MLT pedestal. The beam interaction probability measured with the MLT can be obtained by counting the number of events in the pedestal peak and subtracting this from the total number of counts in the distribution. However, the pedestal peak consists of events where the beam did not interact in the vicinity of the MLT and events where the beam interacted too far away from it. Thus, the MLT values in excess of pedestal reflect only those interactions that took place close to it.

For both the ECD gold peak and MLT pedestal, the number of events within it was determined in the following manner. PAW[11] was used to fit a Gaussian to it, in the range of ADC values over which the particular peak extends. The height, mean, and width of this Gaussian were extracted, and the function was numerically integrated using those parameters. A statistical uncertainty of the integration was calculated using the uncertainties of the fit parameters determined by PAW.

[11]Physics Analysis Workstation, developed by CERN, is a graphical user interface to the HBOOK library of histogram plotting and manipulation tools.

Measurements of the beam's interaction probability were performed on a beam-trigger run that used a 10% target, and one with an empty target. The MLT-pedestal and ECD-gold-peak integrals were performed on distributions obtained with overall average pedestal subtraction, and with the event-by-event pedestal correction described above.

The results of these integrations are shown in Table 2. The ECD data indicates a roughly 31 percent beam interaction probability with the 10% target in place, and a 22 percent interaction probability without it. Comparing these numbers yields a *measured* beam interaction probability with the target of about 11 percent, which is consistent with the 10% target that was used.

The interaction probabilities measured in the MLT data are lower than those from the ECD data, demonstrating the MLT's sensitivity only to interactions close to it. The interaction probability is found to be between 16 and 17 percent with the target in place, and about 8 percent without it. The difference is again 8 to 9 percent, which is consistent with the 10% target used in this run.

pedestal subtraction method	*beam interaction probabilities, percentage*			
	10% target		*empty target*	
	MLT $\neq$ *ped.*	*ECD* $\neq$ *Au*	*MLT* $\neq$ *ped.*	*ECD* $\neq$ *Au*
overall average	16.7±0.6	30.2±0.6	10.9±0.7	21.1±0.7
DSMON-dependent	16.5±0.6	30.6±0.6	8.2±0.7	21.8±0.7

Table 2: Shown here are the measured probabilities of beam interactions, based on the integrals of the ECD gold-signal and MLT pedestal distributions.

The 8 percent probability in the empty-target MLT data implies interactions of the beam in materials close to the MLT but other than the target, such as the collimator. For a perfect detector, this probability, as well as the 22 percent probability seen for empty target data in the ECD, should be zero. This will be investigated in greater detail later in this section.

To attempt to understand the probabilities shown in Table 2, calculations of ^{197}Au interaction probabilities with various materials known to be part of the E896 beamline and detectors were performed. These are now described.

The cross sections of the gold beams' interactions with a given material were assumed to be purely geometric. [13] Such cross sections are described using the formula $\sigma = \pi(R_{Au} + R_{mat})^2$, with $R_{mat} = r_0 A_{mat}^{1/3}$. The radius of the nucleus is R_{mat}, A_{mat} is its atomic weight, and r_0 is in the range from 1.1 to 1.4 fm.

Some materials in the path of the beam are not elemental, such as mylar ($C_5H_4O_2$) and quartz (SiO_2). For these materials, an average atomic weight is calculated from the chemical formula, and used to obtain the geometrical cross section for this material.

The probability of interaction for a given thickness x of the material was then determined from the expression $p(x) = 1 - e^{-\alpha x}$, where $\alpha = \sigma \delta N_{avogadro}/A_{mat}$. The density of the material is δ, and $N_{avogadro}$ is Avogadro's number.

Table 3 shows the results of the calculations of a beam interaction with a particular material in the path of the beam in E896. They are listed in the order in which the

beam approaches these elements. Also shown is the overall interaction probability of the beam up to that point in the beamline.

Calculated interaction probabilities		
beamline element	*individual interaction probability*	*overall interaction probability up to point*
beam counters 400 μm, quartz	0.9 %	0.9 %
BVDs[12]	0.04 %	0.9 %
beam pipe window 5-mill aluminum	0.3 %	1.2 %
SWIC	0.7 %	1.9 %
air—50 cm SWIC to target	0.8 %	2.7 %
target—10% Au	12.1 %	14.5 %
air—1.5 m target to DDC	2.3 %	16.5 %
DDC helium	0.5 %	16.9 %
DDC windows	0.9 %	17.6 %
air—4 m DDC to ECD	6.0 %	22.6 %
ECD quartz 2 mm	4.3 %	25.9 %

Table 3: Shown in the second column are results of the calculations of the probability of the beam's interaction with the materials known to be in the path of the beam. These probabilities were obtained using the geometric cross section and a value of $r_0 = 1.2$ fm. The materials are listed in the order in which the beam ion encounters them in the E896 experimental layout. In the third column are the overall interaction probabilities up to that listed material, calculated as one minus the appropriate product of the individual survival probabilities.

[12]The interaction probability of the beam with the BVD was obtained using an overall thickness of 2 mg/cm^2, [14] and an average A_{mat} appropriate for mylar.

From the BCs to the ECD quartz, the calculated interaction probability is about 26 percent, less than the 31 percent measured in the ECD sum distribution. Thus, there remains a 6 percent interaction probability left unaccounted for. The interactions between the beam and collimator, hinted at by the MLT empty-target data, shall be addressed now, to see if the measured and calculated interaction probabilities can be brought to better agreement. Since beam+collimator interactions should be highly dependent upon the trajectory of the beam, the BVD information will be used to investigate this effect.

For each event, the x and y coordinates of the beam at the two BVDs were calculated, and an extrapolation of the beam trajectory through the measured sweeper magnet fields to the target plane was made. [15] The ECD and MLT signals will be plotted against these beam coordinates on the target, which will be referred to as beam-x and beam-y.

Figure 18 shows the distributions of beam-x and beam-y, along with the value of ECD sum[13] plotted against each beam coordinate. For beam-y above 1.6 cm, there is a greater likelihood of a pedestal value for ECD sum than for a gold-signal value. This implies that the beam is interacting with some material other than the target for these extreme beam-y coordinates. A plot of ECD sum versus beam-y for a narrower range of beam-y is shown in Figure 19; the decrease in ECD sum with an increase in beam-y is obvious.

[13]In compiling ECD sum, the gains were matched, and event-by-event pedestal correction was used.

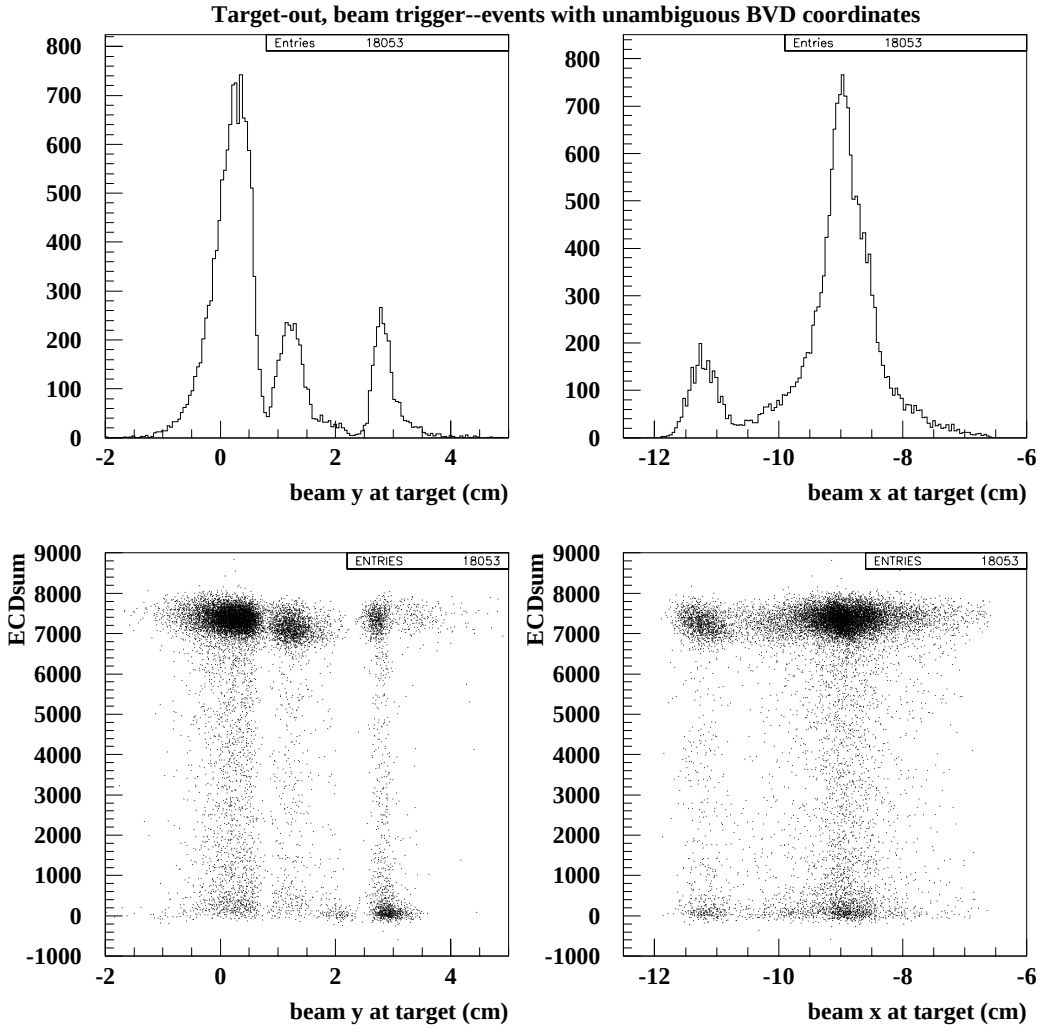

Figure 18: The upper frames show the beam-y and beam-x distributions, respectively, as determined by extrapolating the beam based on the sweeper magnet fields and the BVD data. The lower frames show the dependence of ECD sum (with the pedestal correction algorithm applied) upon the beam's target coordinate. Though no significant dependence of the ECD signals on the beam-x is seen, the ECD signals tend to be more pedestal-like for beam-y greater than about 1.6 cm.

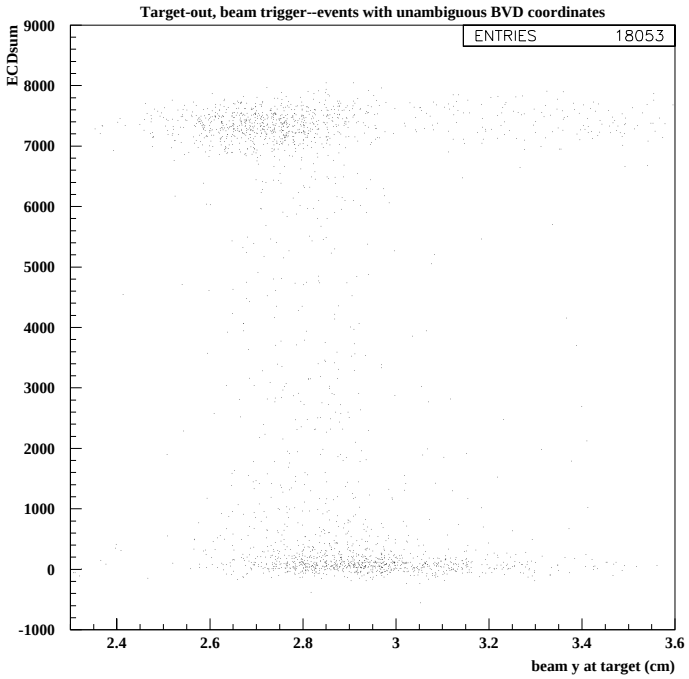

Figure 19: This scatter plot of the ECD sum versus the beam-y coordinate shows quite clearly the overall decrease in ECD with an increase in the height of the beam on the target.

Shown in Figure 20 are the relative sizes of the pedestal and gold-signal peaks of ECD sum for selected ranges of the the beam-y coordinate. Again, there are more counts in the pedestal peak for higher beam locations on target.

The gold-signal peak of the ECD sum distribution was integrated for values of beam-y such that no such collimator clipping was taking place, and the measured interaction probability dropped to 17.8 percent for empty-target events. Comparing this to the calculated interaction probability without the target (15.7 percent) indicates that a 2.5 percent interaction probability remains unaccounted for.

This 2.5 percent discrepancy is close to the $\sim$2 percent errors that arise from the statistical uncertainties in the integrations of the ECD and MLT data, as well as uncertainties in the thicknesses of the beamline materials. Also, there is freedom in the proportionality factor relating R_{mat} to $A_{mat}^{1/3}$, called r_0. If r_0 is taken to be 1.4 fm instead of 1.2 fm, the calculated probability of beam interaction without the target becomes 20.3 percent, which is in excess of the measured value by 3.2 percent.

Figure 21, a plot of MLT sum against the beam-y coordinate, verifies the claim that the collimator, along with a very wide beam profile on target, accounts for much of the non-target interactions. In the same range in beam-y where the position dependent interactions in the ECD data were seen, the MLT response is also increasing.

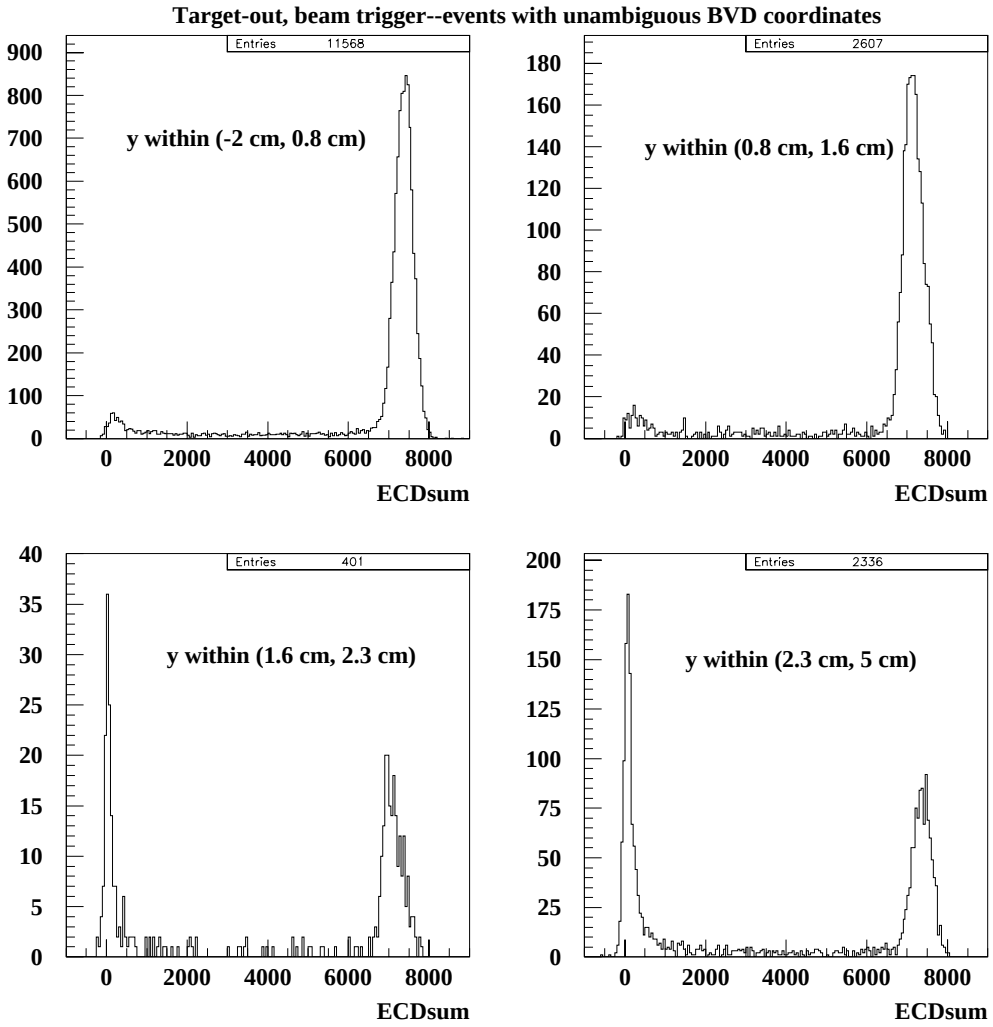

Figure 20: The total ECD signal distributions for various cuts on beam-y. Note that, as the beam-y coordinate range shifts to higher values, the size of the ECD pedestal peak increases relative to the gold-signal peak.

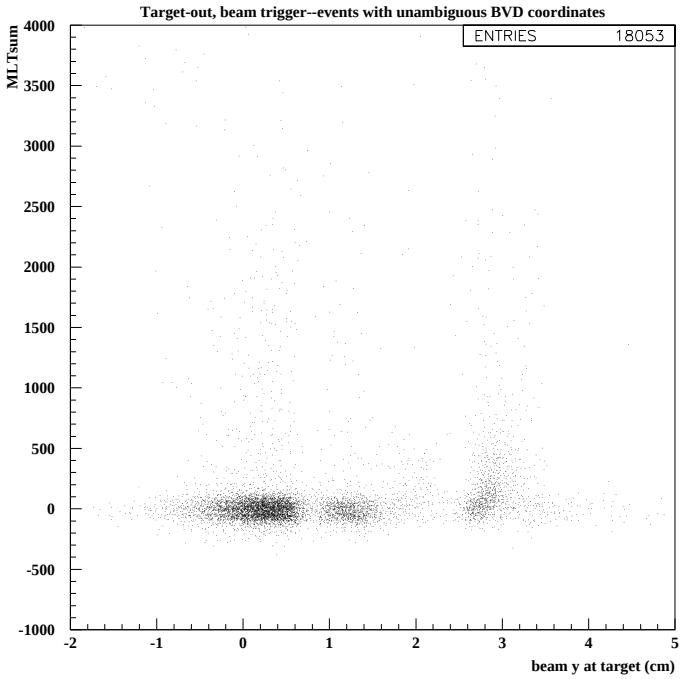

Figure 21: The total MLT signal versus the beam-y. In the same range in beam-y where the decrease in the ECD signal with increasing beam-y was seen, the MLT signal increases with beam-y.

D. Extraction of the impact parameter

With the correlated noise in the ECD and MLT signals accounted for, and the beam interactions explained to some degree, the issue of impact parameter determination in E896 will be addressed.

Figure 16 showed the correlation between the MLT sum and the ECD sum for all events in a 10% target beam-trigger run. It is not obvious from that figure that the identification of an "impact parameter axis" is possible.

Figure 22 shows the correlation between the MLT sum and the ECD sum for interaction events. These are events in which the ECD signal is below the gold peak, and the MLT signal is above its pedestal. The pedestal correction technique has been applied, and those events where the beam struck the collimator were removed using the BVD information. The correlation between these quantities seen in this figure form the impact parameter axis for events measured in E896. The impact parameter is equal to $2R_{Au}$ at the lower right of the figure, and decreases to zero proceeding along this profile toward the upper left. The equivalent impact parameter obtained following cuts on this plot can be obtained using the geometrical prescription described in Reference [13]. According to this prescription, a particular fraction of selected events, f, can be converted to an equivalent impact parameter using the formula $b/b_{max} = \sqrt{f}$, where $b_{max} = 2R_{Au}$.

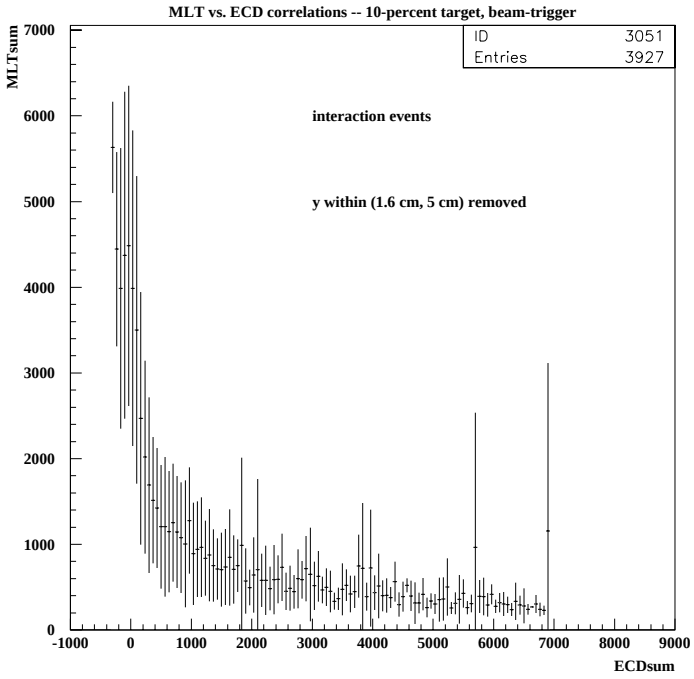

Figure 22: The correlation between MLT sum and ECD sum for interaction events is shown in profile histogram form. Events such that the beam struck the collimator have been removed. As one progresses from the lower right end of the "curve" to the upper left end, the event impact parameter decreases from $2R_{Au}$ to zero.

VI. Conclusion and Outlook

In this Thesis, simulations were described to optimize the design and positioning of the ECD in E896. The height and width of the radiator were set just large enough to intercept those particles with $A/Z \geq 2$. The light-integration volume's dimensions were set just high enough to prevent frequent photocathode hits. The position of the ECD was set using the geometry of the experiment and its magnetic fields.

The ECD was then constructed in such a manner as to diffusely reflect Čerenkov light from a fused quartz radiator, thus making the response independent of hit location. The 8854 PMTs were used because of their good single-photoelectron resolution and their fast rise time, both important qualities for a trigger element.

A look at the raw ECD and MLT data indicated significant correlated noise. To remove this noise offline, an event-by-event pedestal correction technique was used. This correction dramatically narrowed the detector pedestals, as well as the width of the gold-signal peak in the ECD (from 3.3 percent to 2.8 percent). Also, the ECD and MLT data indicated significant probabilities for the interactions of the beam in materials other than the target. These losses were studied via calculations and with searches for events where the ECD and MLT responses depend upon the beam trajectory.

The AGS beam profile is wide, and the study of the ECD and MLT data versus the trajectory of the incident beam indicated unambiguously that extreme beam trajectories hit the E896 collimator. Software cuts were imposed to remove these

extreme beam trajectories. It was then found that the probability for beam interactions in materials other than the target could be described to within 2 percent using calculations based on the geometrical cross section and a parameter r_0 near 1.2 fm.

Overall, the ECD's performance during the January 1997 heavy-ion run was quite satisfactory. The light-collection efficiency was such that the width of the gold-like signal was about 3 percent of the mean, with or without a rigorous event-by-event pedestal correction. This suggests that the light yield from the quartz was sufficient, and that the absorption coefficient of the tyvek was suitably low. Thus, there is no need to modify the ECD light-integration volume before the next gold run, which is scheduled for the spring of 1998.

Prior to the coming run, the rate capability of the PMTs will be improved by adding current amplifiers to stiffen the voltage on the dynodes. The pulse fidelity will also be improved by fabricating negative-high voltage bases, in order to run the photocathode at negative voltage and the anode at ground. With positive-high voltage bases, a coupling capacitor (a high-pass filter) must be placed between the anode and the signal line en route to the ADC, since the anode is at high positive potential. Although the integral of the anode pulse is preserved, the shape of the pulse may not be. If the time constant of the capacitor is too long, then so is the recovery time of the signal line; for a too-short time constant, there will be substantial positive overshoot on the signal line. A negative-high voltage base holds the anode at ground, and thus eliminates the need for a coupling capacitor. [16]

In expectation of the negative-high voltage bases, the PMTs have already been mounted onto the light integration box such that the rim of the aperture in the top and bottom plates is at the same potential as the photocathode. This would get rid of electrostatic effects which might hinder the motion of the first few photoelectrons en route to the first dynode. Figure 23 illustrates this procedure and its effect.

Although the ECD and MLT distributions were narrowed after using the blackened PMT to subtract ECD and MLT pedestals from raw ADC data, the correlations between the blackened PMTs and the ECD and MLT were not optimally "single valued." The blackened PMTs used different signal cable lengths than the ECD and MLT PMTs did, and were read out by a different Fastbus ADC module. Implementing blackened PMTs of the same model as those used on the ECD and MLT, and with similar cable lengths, would be more appropriate. For the ECD, a spare 8854 PMT will be implemented for this purpose.

Finally, attempts will be made to locate the causes of the uncorrelated noise on the experimental floor, and remove them before the next run. Also, to improve the correlation between the ECD and MLT signals, and hence improve the extraction of impact parameters for each event, the ECD and MLT will be operated at higher gains.

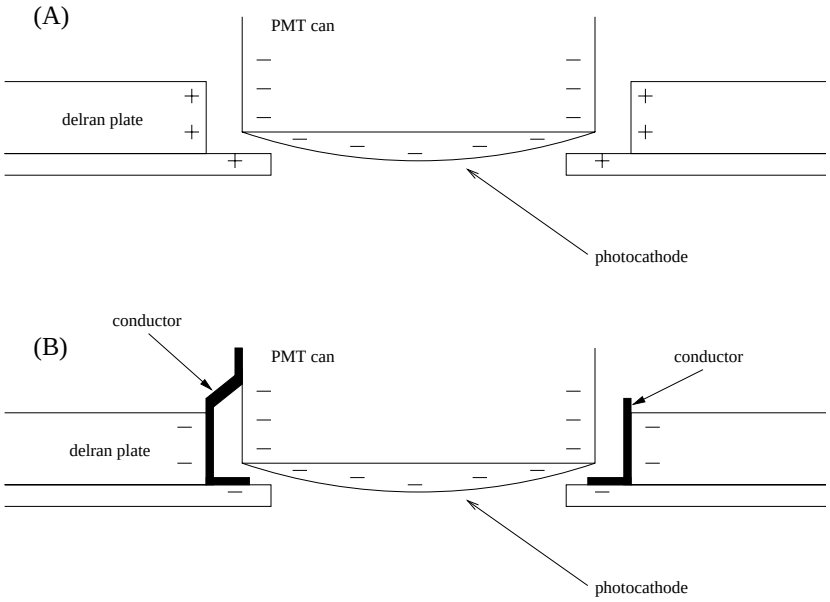

Figure 23: (A) shows that operating the PMTs with a negative-high voltage photocathode may induce a positive charge along the edges of the holes in the Delran plates which accommodate the PMTs. That would set up an electric field which could divert the first few photoelectrons from the first dynode, thus reducing the gain of the PMTs. This can be corrected by placing a conducting strip between the PMT and the Delran rim, as shown in (B).

Bibliography

[1] Stachel, J. and G. R. Young, "Relativistic heavy ion physics at CERN and BNL," *Annu. Rev. Nucl. Part. Sci.*, **42**, 537–597 (1992).

[2] Jaffe, R. L., "Perhaps a Stable Dihyperon," *Phys. Rev. Lett.*, **38**, 195–198 (1977).

[3] Llope, W. J., "The BNL-AGS Experiment 896," *Adv. Nucl. Dynamics 2*, 19–28 (1996).

[4] Kumar, B. S. et al., "High-rate multiplicity detector for relativistic heavy-ion collisions," *Nucl. Inst. Meth. Phys. Res. A*, **357**, 283–291 (1995).

[5] GEANT — *Detector Description and Simulation Tool*, CERN Program Library Long Writeup W5013 (CERN, Geneva, 1993).

[6] Paganis, S. (UT-Austin), private communication.

[7] Shor, A. and R. Longacre, "Effects of secondary interactions in proton-nucleus and nucleus-nucleus collisions using the HIJET event generator," *Phys. Lett. B*, **218**, 100–104 (1989).

[8] Longacre, R. (BNL), private communication.

[9] The expression for Čerenkov energy loss is derived in the course of performing a correct calculation of the density correction to the Bethe-Bloch energy-loss expression. See J. D. Jackson, *Classical Electrodynamics*, 2nd ed., Chap. 13 for details.

[10] RCA Electronic Components, 8854 Photodetector data sheet.

[11] Mitchell, J. W. (NASA GSFC), private communication.

[12] Corning Optical, UV-grade Fused Quartz Code 7940 data sheet.

[13] Cavata, C. et al., "Determination of the impact parameter in relativistic nucleus-nucleus collisions," *Phys. Rev. C*, **42**, 1760–1763 (1990).

[14] Debbe, R. (BNL), private communication.

[15] Milosevich, Z. (CMU), private communication.

[16] Leo, W. R., *Techniques for Nuclear and Particle Physics : a How-to Approach*, 2nd Revised Edition, 187–188 (Springer-Verlag, Berlin, 1994).